Science Advances
AAAS

Supplementary Materials for

Engineered ACE2-Fc counters murine lethal SARS-CoV-2 infection through direct neutralization and Fc-effector activities

Yaozong Chen *et al.*

Corresponding author: Marzena Pazgier, marzena.pazgier@usuhs.edu

Sci. Adv. **8**, eabn4188 (2022)
DOI: 10.1126/sciadv.abn4188

This PDF file includes:

Table S1. Summary of SPR kinetic constants

Protein ID	Immobilized ligand	Flow antigen	Fitting mode	k_{on} ×10^4 ($M^{-1}\cdot s^{-1}$)	k_{off} ×10^{-3} (s^{-1})	K_D (nM)	Chi^2 value
ACE2 (18-615)-Fc							
M27	Wild-type	SARS-CoV-2 RBD	1:1	5.59	1.45	26.0	0.35
		RBD (B.1.1.7)	1:1	16.7	4.14	24.8	0.67
		RBD (B.1351)	1:1	32.3	3.73	11.6	0.66
		SARS-CoV-1 RBD	1:1	45.7	57.5	126	1.61
		SARS-CoV-2 S-6P	1:1	30.4	0.56	1.82	2.74
M33	H374A+H378A	SARS-CoV-2 RBD	1:1	5.91	1.63	27.6	0.48
		RBD (B.1.1.7)	1:1	24.9	5.86	23.6	1.43
		RBD (B.1351)	1:1	46.5	3.58	7.7	0.26
		SARS-CoV-1 RBD	1:1	48.3	56.0	116	3.05
		SARS-CoV-2 S-6P	1:1	30.4	0.57	1.88	1.83
M38	L79F+M82Y	SARS-CoV-2 RBD	1:1	63.7	2.98	4.67	0.72
		RBD (B.1.1.7)	1:1	64.6	5.19	8.02	0.85
		RBD (B.1351)	1:1	114	4.35	3.82	0.47
		SARS-CoV-1 RBD	1:1	199	19.0	9.55	4.12
		SARS-CoV-2 S-6P	1:1	33.7	0.198	0.587	2.33
M39	F28S+K31R	SARS-CoV-2 RBD	1:1	4.27	2.72	63.61	1.45
		RBD (B.1.1.7)	1:1	11.3	10.1	89.8	0.96
		RBD (B.1351)	1:1	14.4	10.8	75.5	1.37
		SARS-CoV-1 RBD	1:1	N.D.			
		SARS-CoV-2 S-6P	1:1	N.D.			
M40	L45D	SARS-CoV-2 RBD	1:1	49.0	9.63	19.66	1.01
		RBD (B.1.1.7)	1:1	15.2	5.25	34.61	0.59
		RBD (B.1351)	1:1	25.6	7.26	28.39	1.01
		SARS-CoV-1 RBD	1:1	N.D.			
		SARS-CoV-2 S-6P	1:1	19.5	0.34	1.76	0.73
M41	Q325Y	SARS-CoV-2 RBD	1:1	42.5	3.88	9.14	0.84
		RBD (B.1.1.7)	1:1	37.6	4.45	11.82	0.83
		RBD (B.1351)	1:1	15.8	1.83	7.95	2.03
		SARS-CoV-1 RBD	1:1	82.4	70.9	86	0.23
		SARS-CoV-2 S-6P	1:1	19.6	0.42	2.14	1.56
M86	L79F+M82Y+Q325	SARS-CoV-2 RBD	1:1	102	3.64	3.58	0.60

	Y+H374A+H378A LFMYQY2HA (GASDALIE-Fc)	RBD (B.1.1.7)	1:1	105	5.04	4.78	0.56
		RBD (B.1351)	1:1	110	1.75	1.59	0.53
		SARS-CoV-1 RBD	1:1	143	18.5	12.9	0.08
		SARS-CoV-2 S-6P	1:1	37.0	0.197	0.533	2.39
ACE2 (18-740)-Fc							
M31	wild type	SARS-CoV-2 RBD	1:1	43.3	6.0	13.9	1.08
		RBD (B.1.1.7)	1:1	19.9	3.61	18.1	0.49
		RBD (B.1351)	1:1	33.0	2.77	8.38	0.29
		SARS-CoV-1 RBD	1:1	72.2	48.0	66.5	0.34
		SARS-CoV-2 S-6P	1:1	12.9	0.13	1.02	1.23
M58	L79F+M82Y+Q325Y+ H374A+H378A LFMYQY2HA (LALA-Fc)	SARS-CoV-2 RBD	1:1	84.6	2.83	3.35	1.26
		RBD (B.1.1.7)	1:1	11.34	4.21	3.72	1.02
		RBD (B.1351)	1:1	21.64	2.88	1.33	0.36
		SARS-CoV-1 RBD	1:1	96.4	24.9	25.8	0.34
		SARS-CoV-2 S-6P	1:1	40.9	0.365	0.891	1.51
M79	L79F+M82Y+Q325Y+ H374A+H378A LFMYQY2HA (IgG3-Fc)	SARS-CoV-2 RBD	1:1	59.6	2.96	4.98	1.82
		RBD (B.1.1.7)	1:1	38.9	6.21	16.0	1.01
		RBD (B.1351)	1:1	71.0	3.39	4.77	0.37
		SARS-CoV-1 RBD	1:1	107	23.6	22.1	0.41
		SARS-CoV-2 S-6P	1:1	49.9	0.347	0.69	1.45
M81	L79F+M82Y+Q325 Y+H374A+H378A LFMYQY2HA (GASDALIE-Fc)	SARS-CoV-2 RBD	1:1	81.8	2.24	2.74	1.51
		RBD (B.1.1.7)	1:1	125	3.62	2.89	12.5
		RBD (B.1351)	1:1	174	1.51	0.87	17.3
		SARS-CoV-1 RBD	1:1	111	19.3	17.4	0.50
		SARS-CoV-2 S-6P	1:1	43.4	0.33	0.76	0.96
	SARS-CoV-2 S RBD (319-591)-Fc	Monomeric $ACE2_{615}$-wild type	1:1	11.1	9.73	87.6	0.66
		Monomeric $ACE2_{615}$-LFMYQY2HA	1:1	48.7	5.82	11.9	0.19

Table S2. Crystallographic data collection and refinement statistics.

	$ACE2_{615}$ (LFMYQY2HA)-RBD
Data collection	
Wavelength, Å	0.979
Resolution range, Å	47.51 - 3.54 (3.667 - 3.54)
Space group	$P2_1$
Unit cell parameter	
a, b, c, Å	132.6, 136.3, 132.7
α, β, γ, °	90.0, 92.5, 90.0
Redundancy	22.1 (3.0)
Completeness, %	96.98 (91.52)
Mean I/sigma(I)	4.71 (1.23)
R_{merge}[a]	0.151 (0.804)
R_{pim}[b]	0.140 (0.896)
$CC_{1/2}$[c]	0.899 (0.447)
Wilson B_{factor}, ($1/Å^2$)[d]	108.39
Refinement	
R_{work}[e]	0.245 (0.362)
R_{free}[f]	0.292 (0.411)
Resolution, Å	47.51 - 3.54
# of non-hydrogen atoms	
proteins	25351
water	3
Overall B_{factor}, ($Å^2$)	
proteins	122.75
ligands	126.05
water	37.15
RMS (bond lengths), Å	0.004
RMS (bond angles), °	0.69
Ramachandran[g]	
Favored, %	96.35
Allowed, %	3.61
Outliers, %	0.03
PDB ID	7RPV

Statistics for the highest-resolution shell are shown in parentheses.

[a] $R_{merge} = \sum | I - \langle I \rangle | / \sum I$, where I is the observed intensity and $\langle I \rangle$ is the average intensity obtained from multiple observations of symmetry-related reflections after rejections

[b] R_{pim} = as defined in (*68*).

[c] $CC_{1/2}$ = as defined by Karplus and Diederichs (*69*)

[d] Wilson B_{factor} as calculated in (*70*)

[e] $R = \sum \| F_o | - | F_c \| / \sum | F_o |$, where F_o and F_c are the observed and calculated structure factors, respectively.

[f]R_{free} = as defined by Brünger (*71*)
[g]Calculated with MolProbity (*72*).

Table S3. Sequences of the real time PCR primers

Target gene	Forward	Reverse
PsV *ZsGreen*	GACAGATAACTGGGAGCCATCC	CGGCATCTTTCTTGGCACAGAC
SARS-CoV-2 *N*	ATGCTGCAATCGTGCTACAA	GACTGCCGCCTCTGCTC
Mouse *Il1b*	GCCACCTTTTGACAGTGATGAG	CTCCTCTTCGCACTTCTGCTC
Mouse *Il6*	TAGTCCTTCCTACCCCAATTTCC	GACAGCCCAGGTCAAAGGTT
Mouse *Tnfa*	CCACCACGCTCTTCTGTCTAC	AGGGTCTGGGCCATAGAACT
Mouse *Ifng*	ATGAACGCTACACACTGCATC	CCATCCTTTTGCCAGTTCCTC
Mouse *Actin*	GGCTGTATTCCCCTCCATCG	CCAGTTGGTAACAATGCCATGT

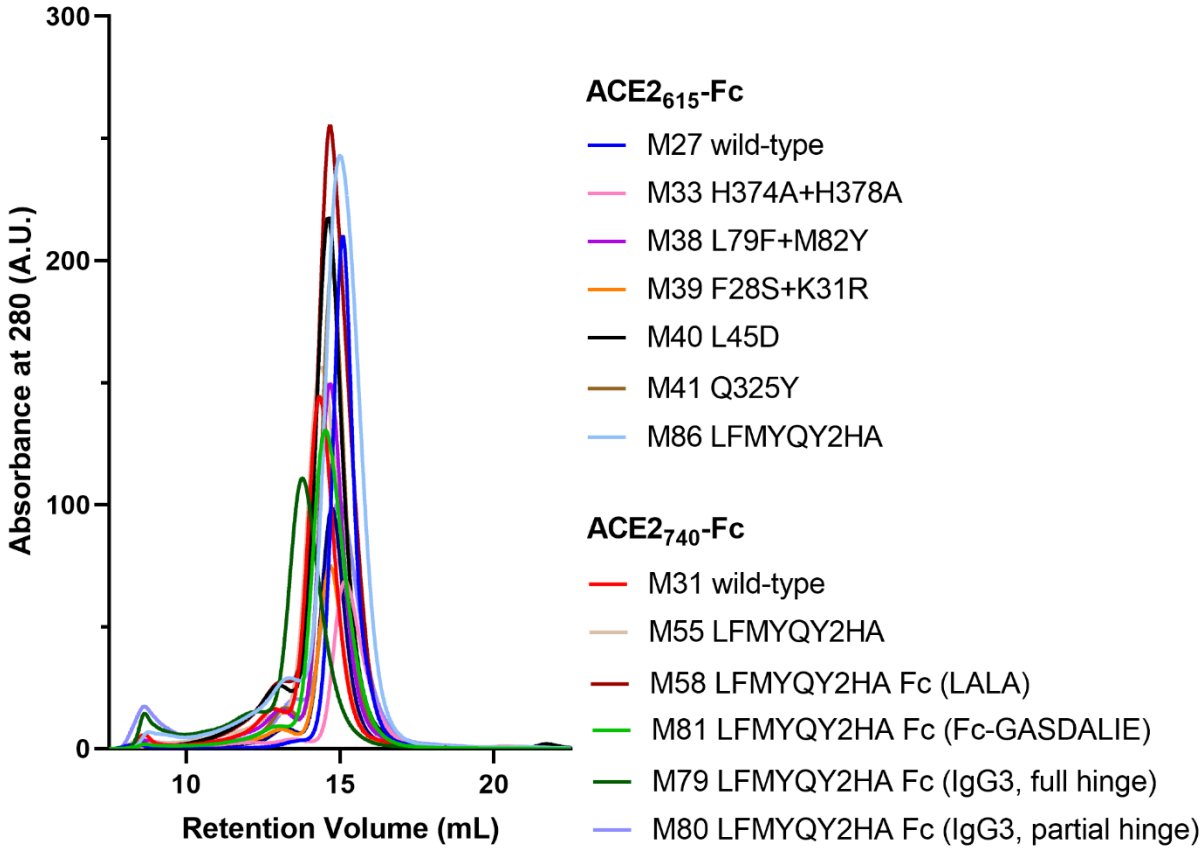

Fig. S1. Size exclusion chromatographic (SEC) profiles of purified ACE2-Fc variants.

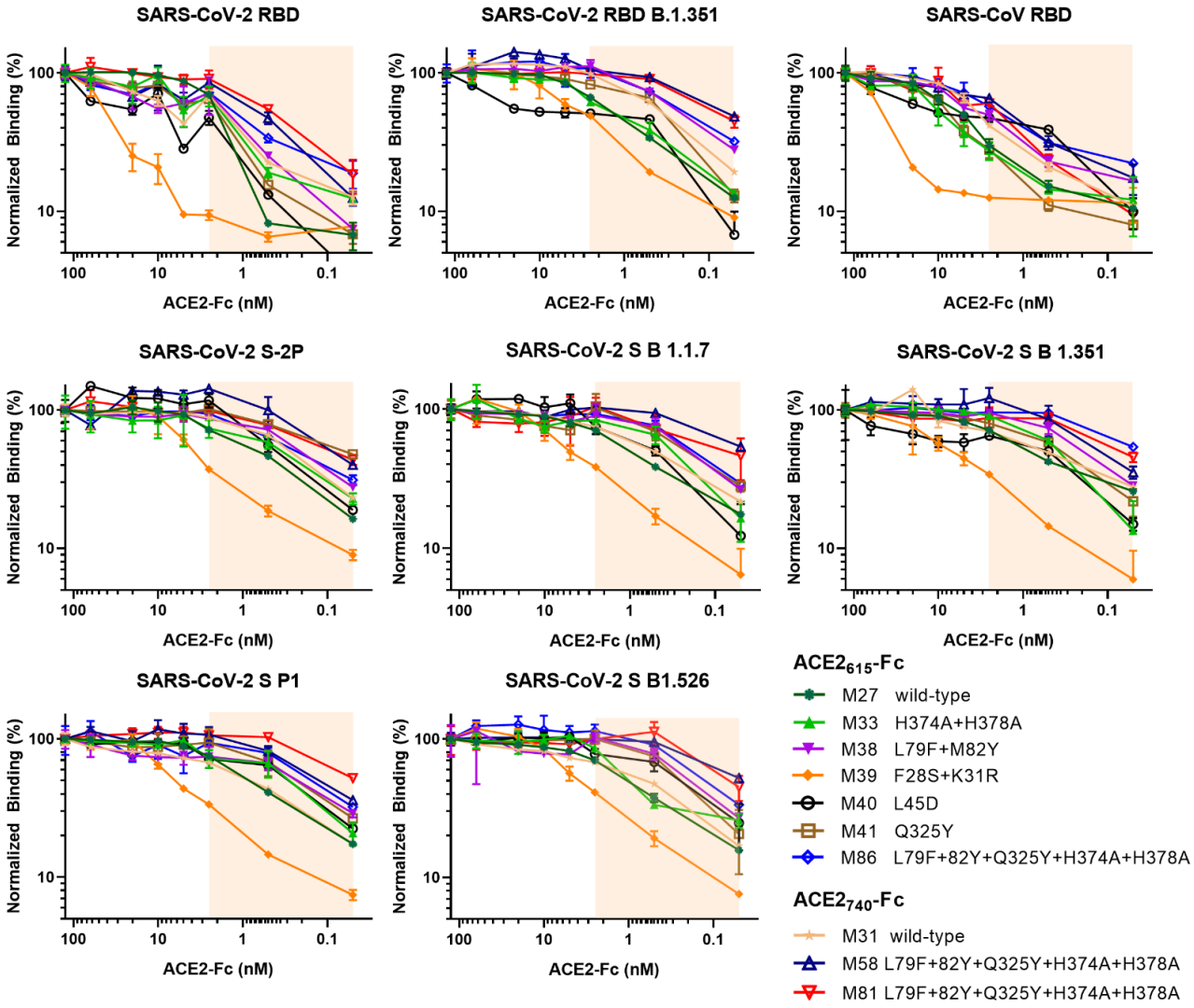

Fig. S2. ELISA binding of ACE2-Fc variants to SARS-CoV-2 and SARS-CoV-1 antigens. Related to Fig. 2D. Serial dilutions (0.05-125 nM) of purified ACE2-Fcs were applied to each well pre-coated with 50 ng of SARS-CoV-2 RBD, $RBD_{B1.351}$, SARS-CoV-1 RBD or 75 ng of SARS-CoV-2 S-2P, $S_{B.1.1.7}$, $S_{B.1.351}$, SP.1, $S_{B.1.526.}$ AUCs in the unsaturated region (0.05-2.50 nM, shaded in wheat) were calculated, normalized (binding at 125nM set as 100%) and plotted as heat-map shown in **Fig. 2D**.

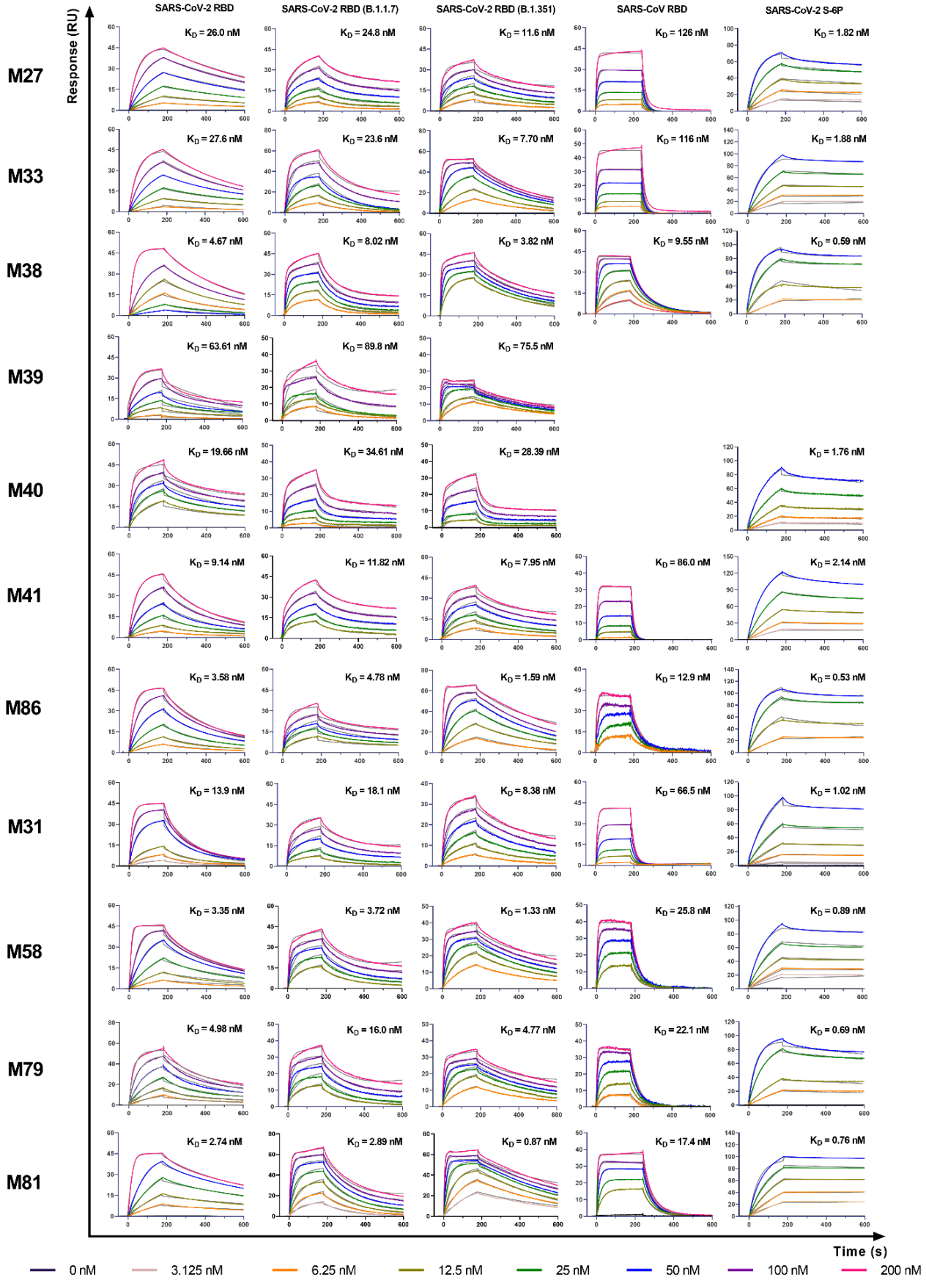
SARS-CoV-2 RBD
SARS-CoV-2 RBD (B.1.1.7)
SARS-CoV-2 RBD (B.1.351)
SARS-CoV RBD
SARS-CoV-2 S-6P
M27
M33
M38
M39
M40
M41
M86
M31
M58
M79
M81
Response (RU)
K_D = 26.0 nM
K_D = 24.8 nM
K_D = 11.6 nM
K_D = 126 nM
K_D = 1.82 nM
K_D = 27.6 nM
K_D = 23.6 nM
K_D = 7.70 nM
K_D = 116 nM
K_D = 1.88 nM
K_D = 4.67 nM
K_D = 8.02 nM
K_D = 3.82 nM
K_D = 9.55 nM
K_D = 0.59 nM
K_D = 63.61 nM
K_D = 89.8 nM
K_D = 75.5 nM
K_D = 19.66 nM
K_D = 34.61 nM
K_D = 28.39 nM
K_D = 1.76 nM
K_D = 9.14 nM
K_D = 11.82 nM
K_D = 7.95 nM
K_D = 86.0 nM
K_D = 2.14 nM
K_D = 3.58 nM
K_D = 4.78 nM
K_D = 1.59 nM
K_D = 12.9 nM
K_D = 0.53 nM
K_D = 13.9 nM
K_D = 18.1 nM
K_D = 8.38 nM
K_D = 66.5 nM
K_D = 1.02 nM
K_D = 3.35 nM
K_D = 3.72 nM
K_D = 1.33 nM
K_D = 25.8 nM
K_D = 0.89 nM
K_D = 4.98 nM
K_D = 16.0 nM
K_D = 4.77 nM
K_D = 22.1 nM
K_D = 0.69 nM
K_D = 2.74 nM
K_D = 2.89 nM
K_D = 0.87 nM
K_D = 17.4 nM
K_D = 0.76 nM
Time (s)
0 nM
3.125 nM
6.25 nM
12.5 nM
25 nM
50 nM
100 nM
200 nM

Fig. S3. SPR kinetic measurement of SARS-CoV-2/SARS-CoV antigens binding to immobilized ACE2-Fcs. Related to Fig. 2F and Table S2. All measurement were performed on a Protein A chip with ACE2-Fc immobilized to different levels according to the flow antigens: ~80-200 RU for SARS-CoV-2 RBD, $RBD_{B.1.1.7}$ and $RBD_{B.1.351}$, ~120 RU for SARS-CoV-1 RBD and ~60 RU for SARS-CoV-2 non-tagged S-6P. The flow antigens were injected at indicated concentrations. The background-corrected sensorgrams (colored) were fitted with 1:1 Langmuir model (grey) and the kinetic constants were summarized in **Table S1.**

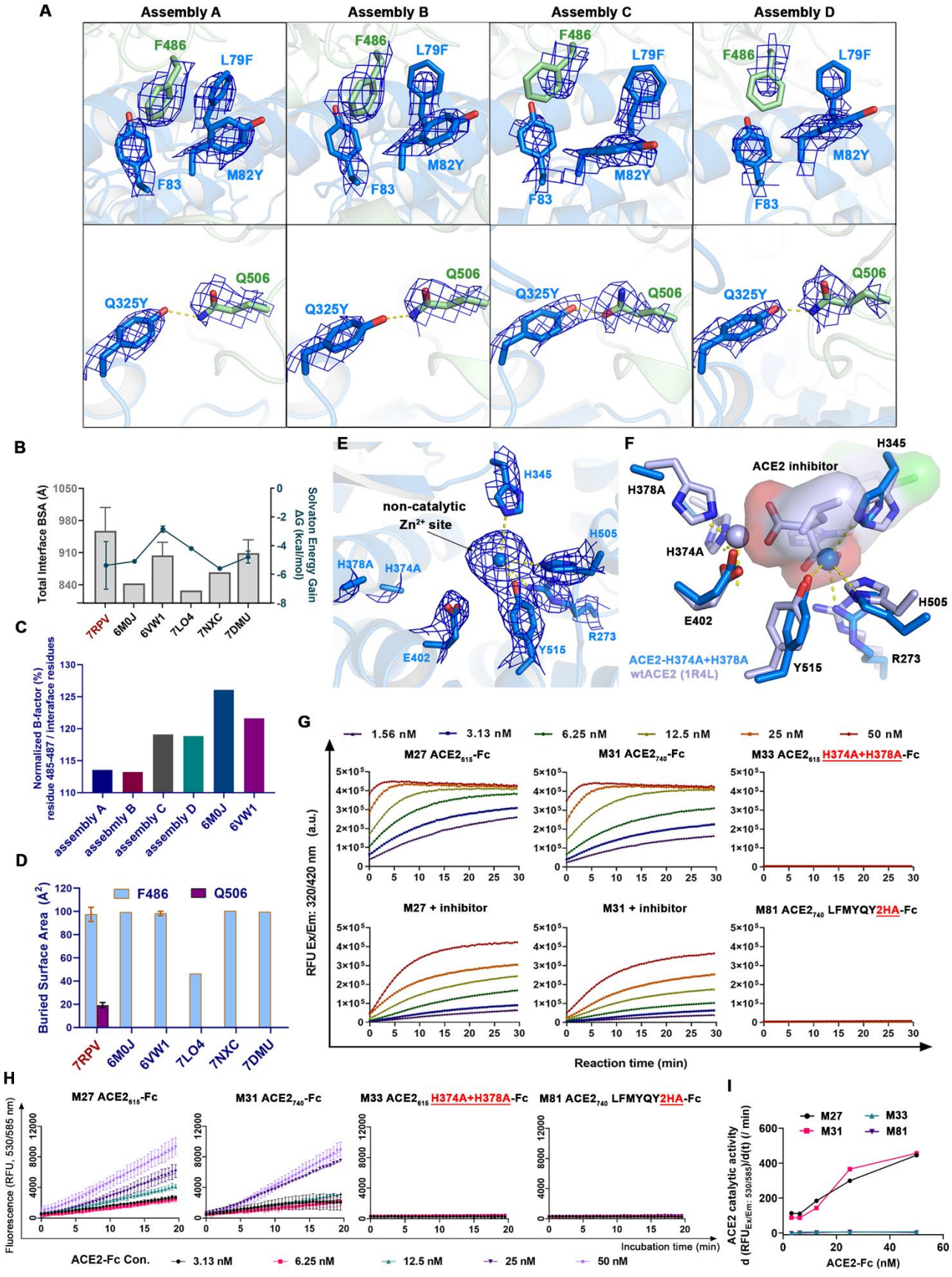
A
Assembly A
Assembly B
Assembly C
Assembly D
F486
L79F
F83
M82Y
Q325Y
Q506
B
Total Interface BSA (Å)
Solvation Energy Gain ΔG (kcal/mol)
7RPV
6M0J
6VW1
7LO4
7NXC
7DMU
C
Normalized B-factor (%) residue 485-487 / interaface residues
assembly A
assebmly B
assembly C
assembly D
6M0J
6VW1
D
Buried Surface Area (Å²)
F486
Q506
E
H345
non-catalytic Zn²⁺ site
H505
H378A
H374A
R273
E402
Y515
F
ACE2 inhibitor
H345
H378A
H374A
E402
H505
R273
Y515
ACE2-H374A+H378A
wtACE2 (1R4L)
G
1.56 nM
3.13 nM
6.25 nM
12.5 nM
25 nM
50 nM
M27 ACE2615-Fc
M31 ACE2740-Fc
M33 ACE2615 H374A+H378A-Fc
M27 + inhibitor
M31 + inhibitor
M81 ACE2740 LFMYQY2HA-Fc
RFU Ex/Em: 320/420 nm (a.u.)
Reaction time (min)
H
M27 ACE2615-Fc
M31 ACE2740-Fc
M33 ACE2615 H374A+H378A-Fc
M81 ACE2740 LFMYQY2HA-Fc
Fluorescence (RFU, 530/585 nm)
Incubation time (min)
ACE2-Fc Con.
3.13 nM
6.25 nM
12.5 nM
25 nM
50 nM
I
M27
M31
M33
M81
ACE2 catalytic activity d (RFUEx/Em: 530/585)/d(t) (/ min)
ACE2-Fc (nM)

Fig. S4. Crystal structure of engineered ACE2$_{615}$ LFMYQY2HA in complex with SARS-CoV-2 RBD. Related to Fig. 3. (**A**) $2F_o$-F_c electron density map (contour level = 1.0 σ) of affinity-enhancing mutations L79F, M82Y and Q325Y in four assemblies within the ASU. (**B**) Total buried surface area (BSA) of -ACE2-RBD interface and solvation energy gain upon complex formation analyzed for ACE2$_{615}$ LFMYQY2HA-RBD, four wtACE2-RBD complexes (PDB: 6M0J, 6VW1, 7LO4, 7NXC) and ACE2-RBD complex where ACE2 was mutated to gain enhanced RBD affinity (PDB: 7DMU). (**C**) Normalized average B-factor of RBD ridge residues 485-487 to those of the respective ACE2-RBD interface residues among the four assemblies of ACE2$_{615}$ LFMYQY2HA-RBD structure and two wtACE2-RBD crystal structures. Interface residues were defined as those with BSA>0 Å^2 when calculated in PISA. (**D**) Buried surface area of two RBD residues F486 and Q506 among ACE2-RBD complexes. (**E**) $2F_o$-F_c electron density map (contour level = 1.0 σ) of the active site residues in ACE2$_{615}$ LFMYQY2HA. (**F**) Active site superimposition of ACE2$_{615}$ LFMYQY2HA and wtACE2 bound to inhibitor MLN-4760. Molecular surface is displayed over the inhibitor molecule and the coordinating residues are shown as sticks. (**G**) Time course measurement of ACE2 enzyme activity. The slopes of the initial linear region were calculated and plotted as **Fig. 3G**. (**H**) ACE2 activity assay using Ang II peptide as substrate, coupled with phenylalanine detection kit. The selected ACE2-Fc, M27, M31, M33 or M81 was added to the pre-mixed AngII and coupling enzymes at indicated concentrations. (**I**) Summary of the ACE2 enzyme activity shown in (**H**). The slopes of the initial linear region of the reaction, as reflected by the fluorometric product formation, were plotted against the indicated ACE2-Fc concentrations.

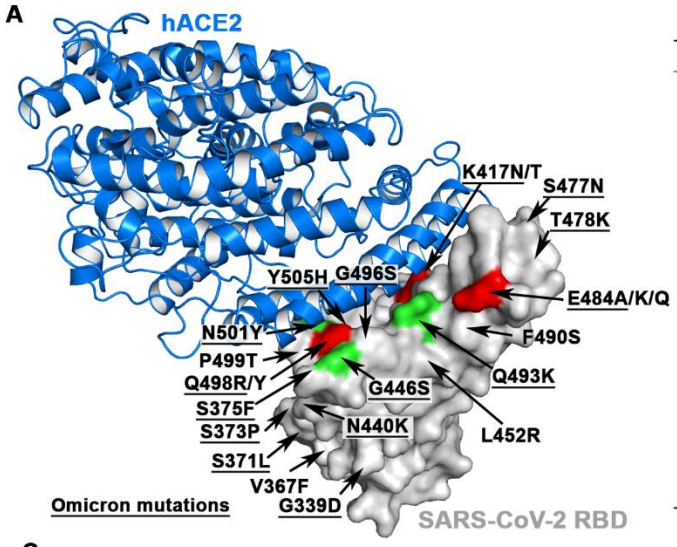

B

WHO names (Pango names)	RBD mutations (favor, neutral, adverse)
Alpha (B.1.1.7)	N501Y
Beta (B.1.351)	K417N/E484K/N501Y
Gamma (P1 or B.1.1.28)	K417T/E484K/N501Y
Delta (B.1.617.2)	(K417N)/L452R/T478K
Epsilon (B1.427)	L452R
Zeta (B.1.1.28.2) or Eta (B.1.525)	E484K
Theta (B.1.1.28.3)	E484K/N501Y
Iota (B.1.526)	S477N/E484K
Kappa (B.1.617.1)	L452R/E484Q
Lambda (B.1.1.1.C37)	L452Q/F490S
A.23.1	V367F
Omicron (B.1.1.529)	G339D/S371L/S373P/S375F/K417N/N440K/G446S/S477N/T478K/E484A/Q493K/G496S/Q498R/N501Y/Y505H

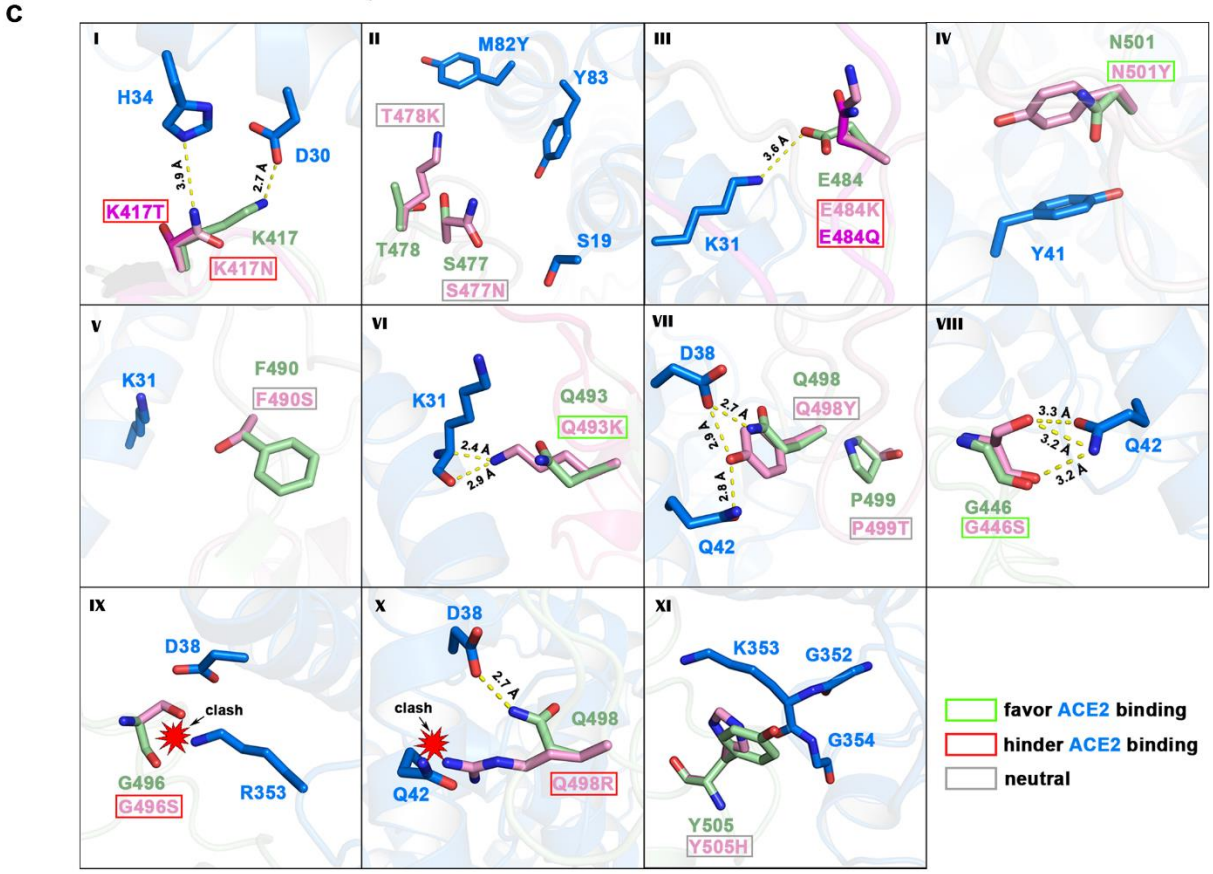

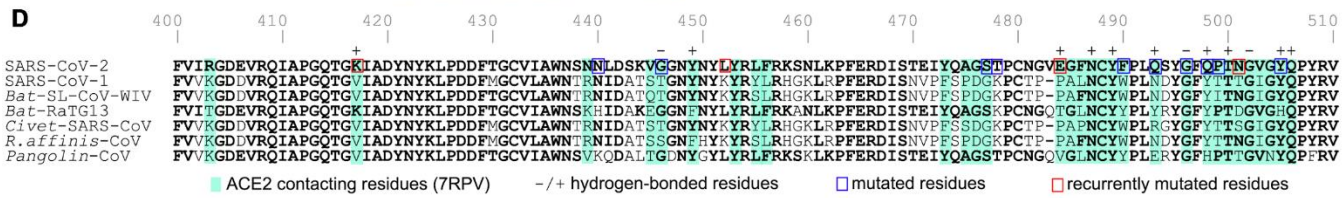

Fig. S5. Structural basis for broad-reactivity against SARS-CoV-2 VOCs. Related to Fig. 3, 4 and 8. (**A-B**) Mapping and summary of the RBD mutations in SARS-CoV-2 VOCs in the context of the mutant ACE2-RBD structure. VOCs mutations that were structurally predicted to be favorable, neutral or deleterious to ACE2 binding are colored in green, grey and red respectively. (**C**) Composite model of RBD mutations on or around the ACE2 binding site. Our structural model provides a rational explanation on the mild VOC resistance to the engineered ACE2-Fc M81. For instance, two RBD hotspot residues K417 and E484, which form salt-bridges with two ACE2 Site-I residues D30 and K31 respectively, are recurrently substituted by K417N/T and E484K/Q in several SARS-CoV-2 VOCs. These mutations abrogate the salt-bridges with ACE2 and therefore are predicted to be deleterious to RBD binding. As expected, $PsV_{B.1.526}$ harboring E484K and $PsV_{B.1.351}$ with K417N and E484K display the highest resistance to M81 (IC_{50} = 2.06 and 1.14 nM respectively, **Fig. 4**) as compared to the PsV_{D614G} (0.23 nM). Another frequently occurred RBD mutant N501Y, as identified in B.1.1.7, B.1.351 and P.1, is thought to enhance the receptor binding by an additional π-π interaction with $Y41_{ACE2}$ and thereby increases the viral infectivity (*73*). However, $PsV_{B.1.1.7}$ with the sole RBD mutation N501Y is less sensitive to M81 (0.52 nM) as compared to PsV_{D614G} (**Fig. 4**), suggesting that prediction of ACE2-Fc cross-reactivity by only considering RBD mutation would be inadequate and mutations in N-terminal domain (NTD) and S2 subunit may affect the sensitivity to the engineered ACE2-Fcs. (**D**) Sequence alignments for receptor binding region of SARS-CoV-2 S with other five coronaviruses that utilize ACE2 as receptor. Contact residues involved in salt-bridges or H-bonds to the $ACE2_{615}$ LFMYQY2HA are marked above the sequence with (+) for the side chain and (-) for the main chain.

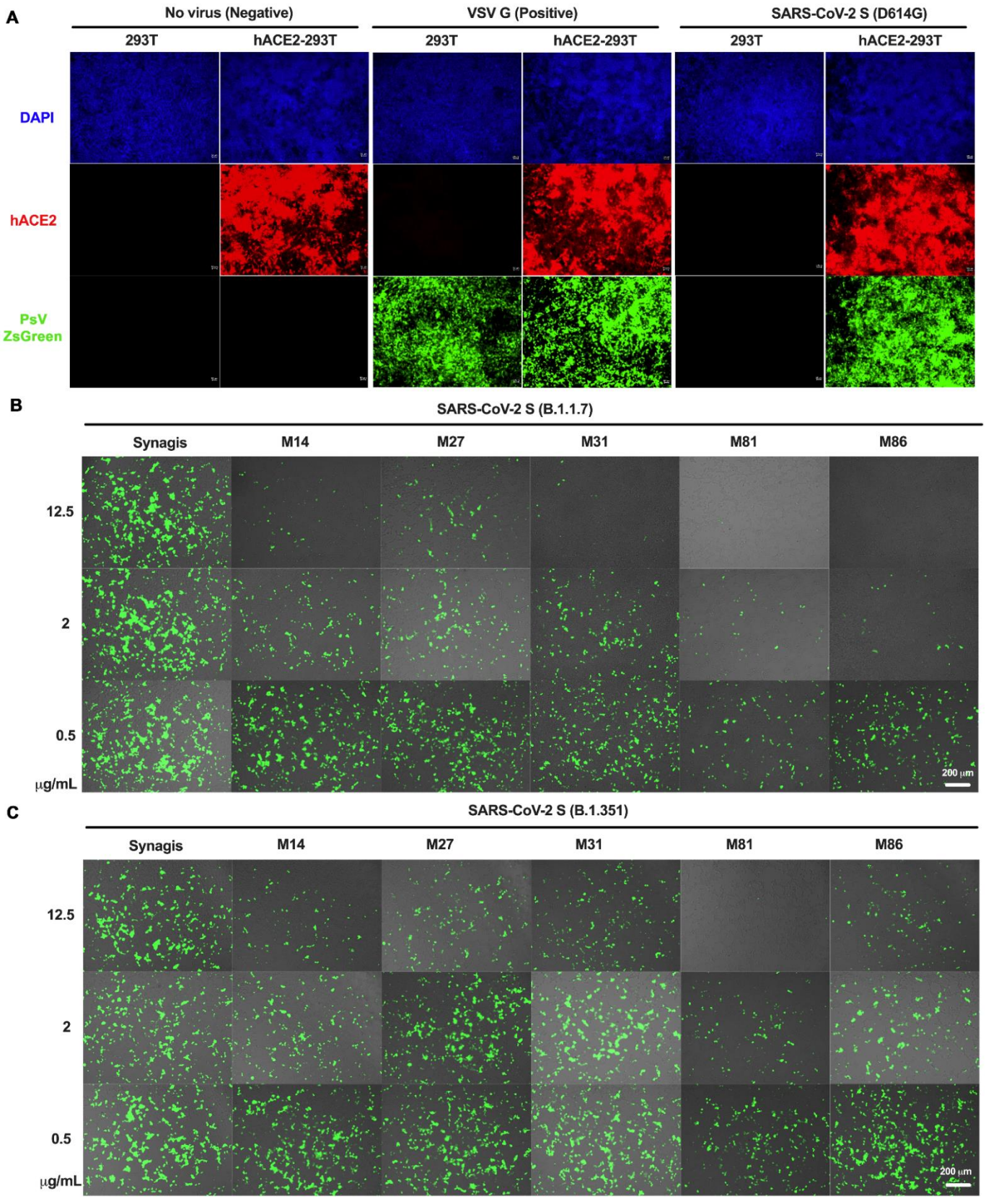
A
No virus (Negative)
VSV G (Positive)
SARS-CoV-2 S (D614G)
293T
hACE2-293T
293T
hACE2-293T
293T
hACE2-293T
DAPI
hACE2
PsV ZsGreen
B
SARS-CoV-2 S (B.1.1.7)
Synagis
M14
M27
M31
M81
M86
12.5
2
0.5
μg/mL
200 μm
C
SARS-CoV-2 S (B.1.351)
Synagis
M14
M27
M31
M81
M86
12.5
2
0.5
μg/mL
200 μm

Fig. S6. Engineered ACE2-Fc variants inhibit PsV of SARS-CoV-2 VOCs from infecting hACE2-expressing 293T cells. Related to Fig. 4. (**A**) 293T or hACE2-expressing 293T cells were treated with saline control (no virus), VSV-G PsV (positive control, ~10^5 RLU) or SARS-CoV-2 PsV_{D614G} (~10^6 RLU) carrying ZsGreen reporter gene; ZsGreen signal was detected at 96 h post infection and hACE2 expression was further validated by IF staining (red) using anti-hACE2 antibody. (**B** and **C**) Representative fluorescent imaging of hACE2-expressing 293T cells that were infected with SARS-CoV-2 $PsV_{B.1.1.7}$ (**B**) or $PsV_{B.1.351}$ (**C**) in the presence of indicated concentrations of hACE2-Fc. hACE2-Fc were pre-incubated with PsV for 1 h and the protein-virus mixtures were added to hACE2-expressing 293T cells. Images taken 48h post infection were showed as merged brightfield (cell shape) and greenfield (ZsGreen signal). Scale bar: 200 μm. *n* = 3 replicates/group.

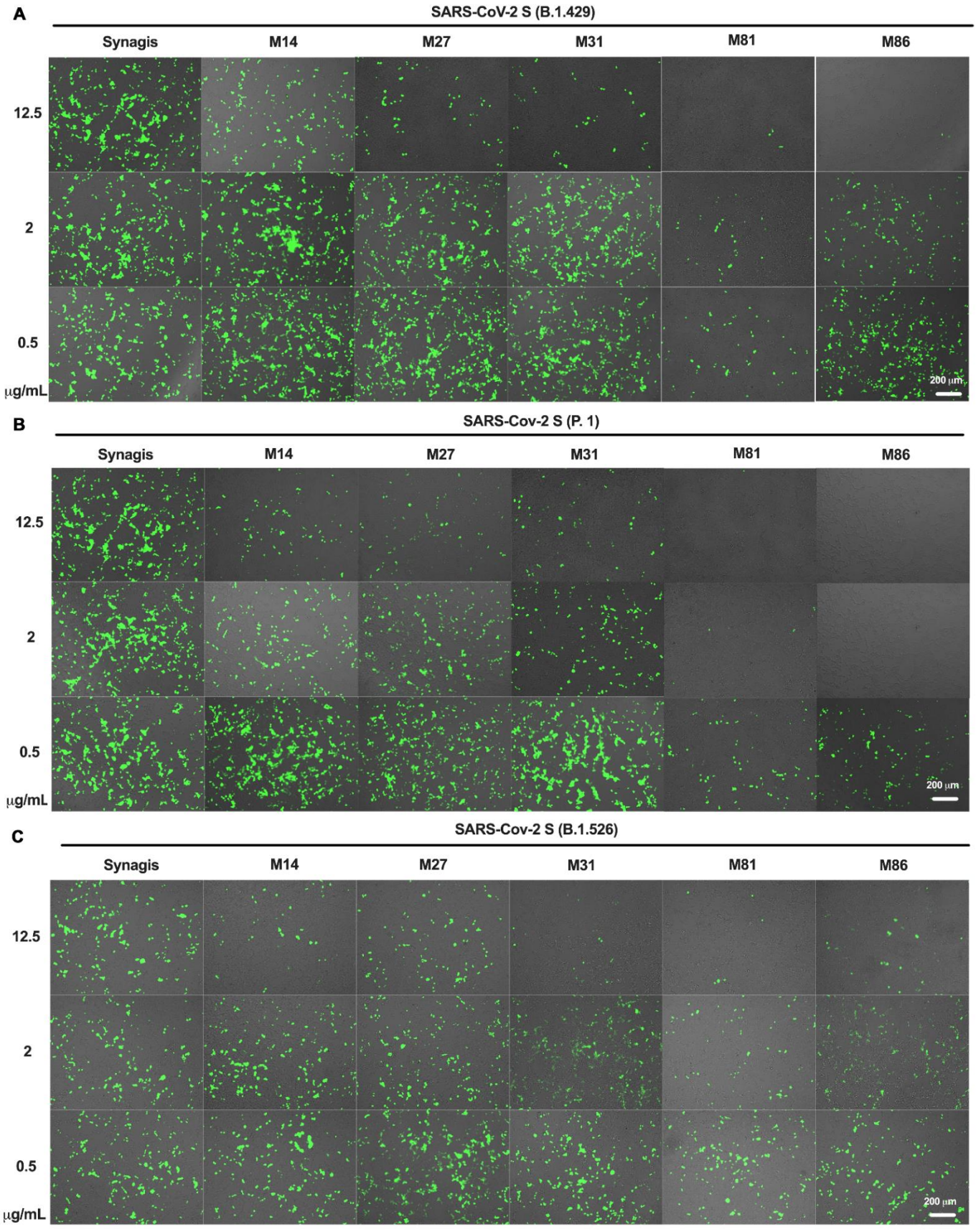
A
SARS-CoV-2 S (B.1.429)
Synagis
M14
M27
M31
M81
M86
12.5
2
0.5
μg/mL
200 μm
B
SARS-Cov-2 S (P. 1)
Synagis
M14
M27
M31
M81
M86
12.5
2
0.5
μg/mL
200 μm
C
SARS-Cov-2 S (B.1.526)
Synagis
M14
M27
M31
M81
M86
12.5
2
0.5
μg/mL
200 μm

Fig. S7. Engineered ACE2-Fc variants inhibit PsV of SARS-CoV-2 VOCs from infecting hACE2-expressing 293T cells. Related to Fig. 4. (A-C) Representative fluorescent imaging of hACE2-expressing 293T cells that were infected with SARS-CoV-2 $PsV_{B.1429}$ (**A**), $PsV_{P.1}$ (**B**) or $PsV_{B.1.526}$ (**C**) in the presence of indicated concentration of ACE2-Fc variants. Experimental procedures and image acquisition were identical as described in **Fig. S6**.

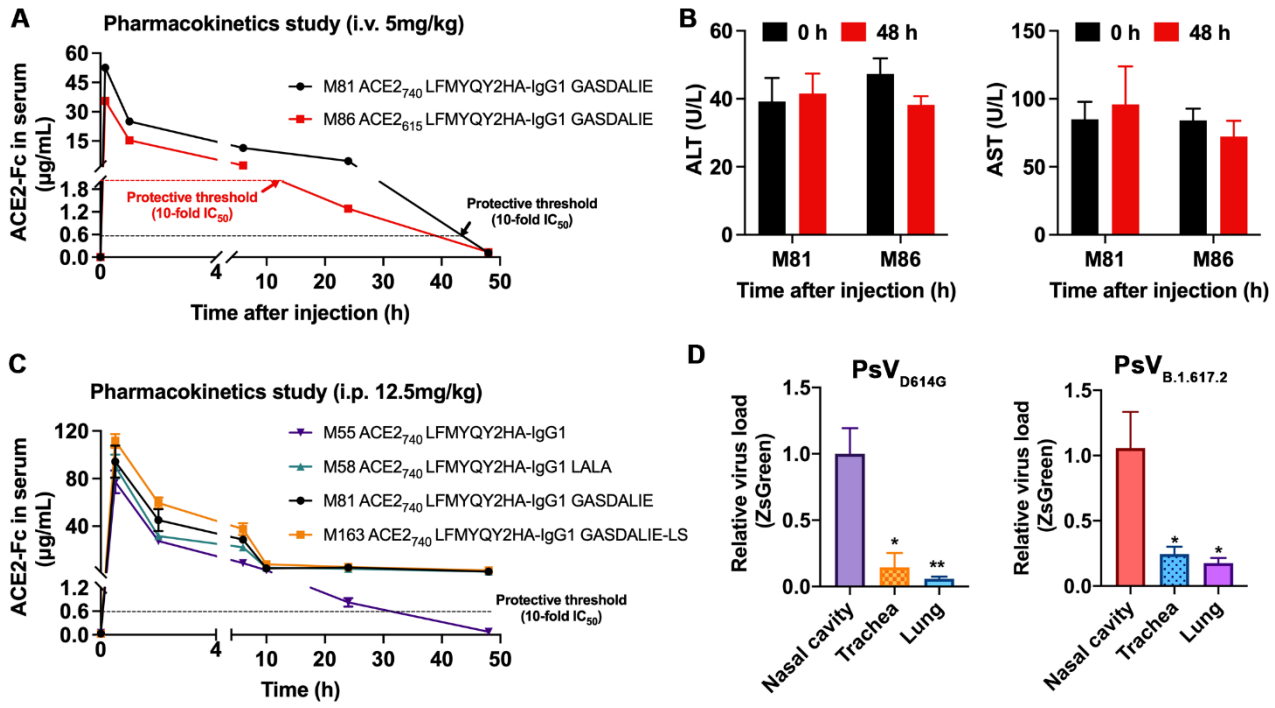

Fig. S8. Pharmacokinetic (PK) study and hepatotoxicity test of two engineered ACE2-Fc. Related to Fig. 5 and Fig. 7. (**A**) C57BL/6J mice were administered by 100 μg (*i.v.*, 5 mg/kg) of two engineered ACE2-Fc variants M81 and M86. Serum samples were collected at 0 min, 10min, 1 h, 6 h, 24 h and 48 h post injection. The ACE2-Fc serum concentrations were determined by indirect ELISA (see Materials and Methods). (**B**) Serum concentrations of alanine transaminase (ALT) and aspartate transaminase (AST) before and 48 h after M81 or M86 injection. n = 3 replicates/group. (**C**) C57BL/6J mice were administered by 375 μg (*i.p.*, 12.5 mg/kg) of engineered ACE2-LFMYQY2HA with wild-type Fc (M55), LALA-Fc (M58), GASDALIE-Fc (M81) and GASDALIE-LS-Fc (LS: M428L/N434S (*74*)). Serum ACE2-Fc concentration was determined as described in (**A**). (**D**) The relative viral loads of nasal cavity, trachea and lung (13 dpi) in PsV-challenged K18-hACE2 mice in the Synagis-treated group (n=3-4). The relative mRNA levels of ZsGreen were calculated as fold change compared to those of nasal cavity. **P*<0.05, ***P*<0.01, versus nasal cavity. The data are shown as means ± the SEM.

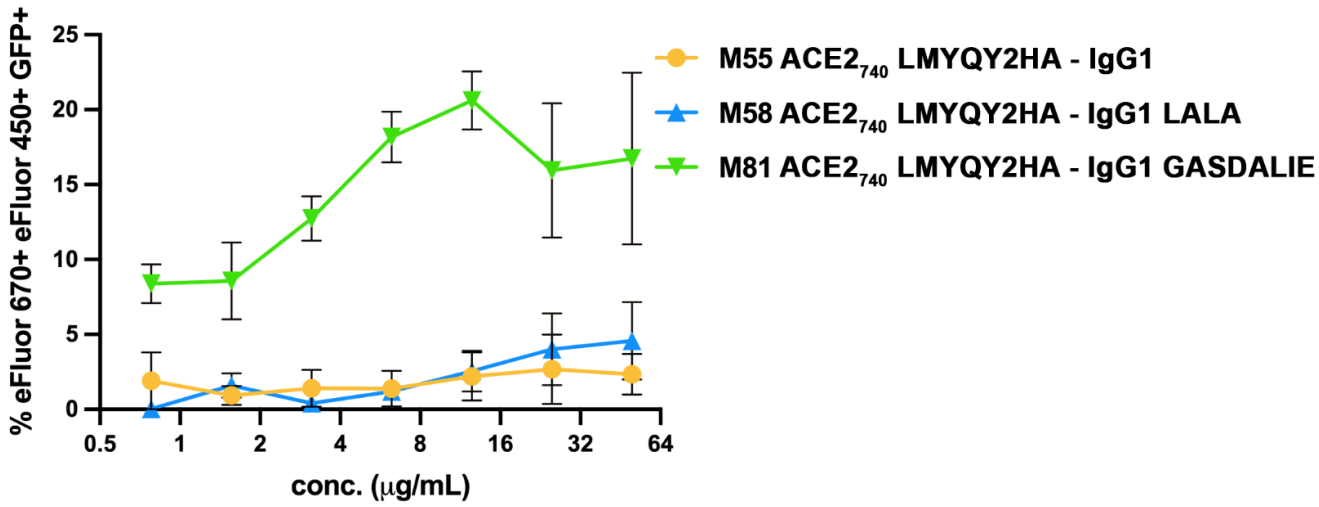

Fig. S9. ACE2-Fc mediated phagocytosis against S-expressing CEM.NKr cells. Related to Fig. 6. Percentage of ADCP in the presence of titrated amounts of ACE2-Fcs using CEM.NKr-Spike cells as targets and THP-1 cells as phagocytic effectors cells. Data are the average from 3 experiments; mean values ± SEM are depicted.

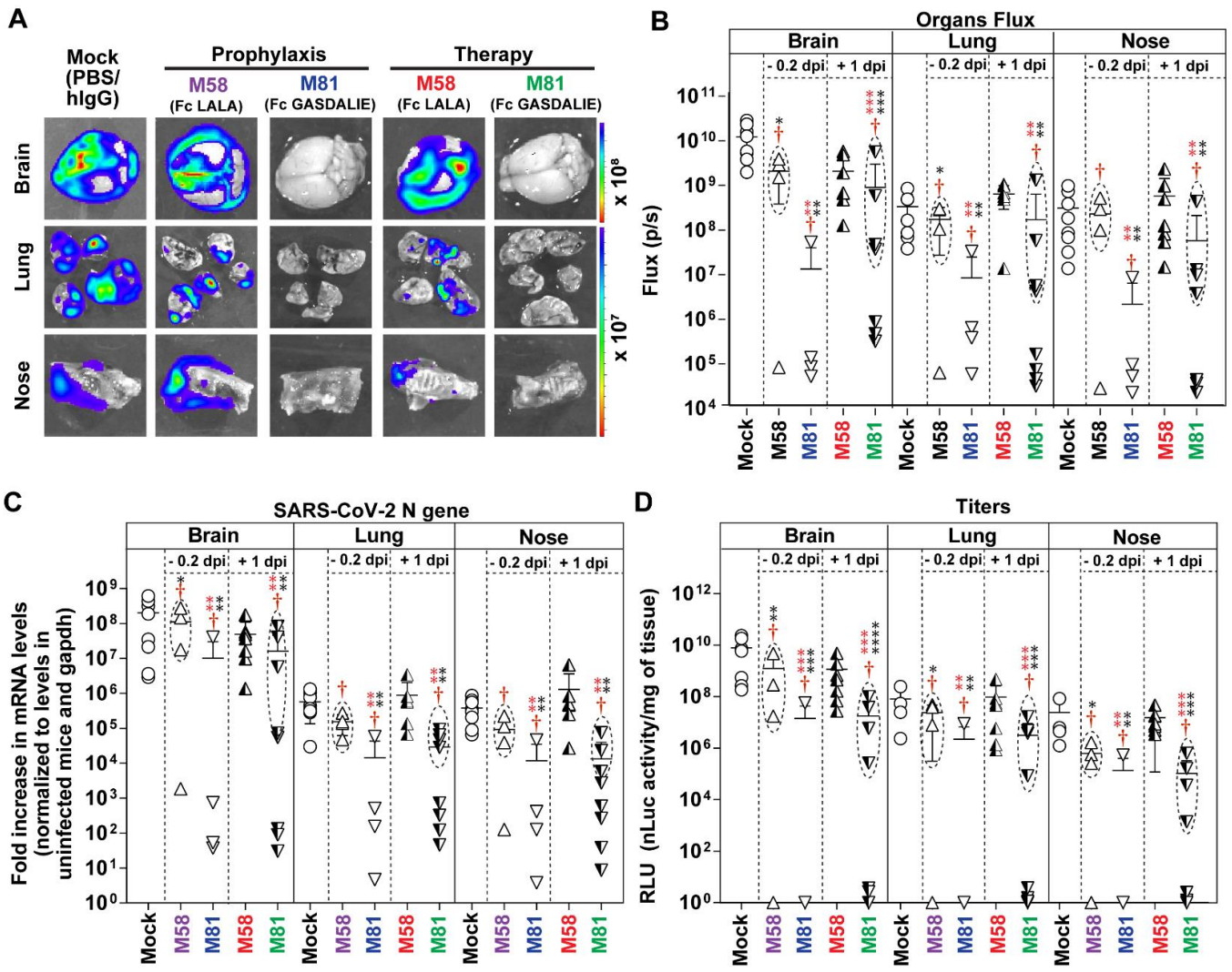

Fig. S10. M81 significantly reduces virus loads in target organs of SARS-CoV-2-nLuc infected K18-hACE2 mice. Related to Fig. 7. (**A-B**) *Ex vivo* imaging of indicated organs and quantification of nLuc signal as flux (photons/sec) after necropsy for an experiment shown in Figure 7. (**C**) Fold changes in nucleocapsid mRNA expression in brain, lung and nasal cavity tissues. Data were normalized to *Gapdh* mRNA in the same sample and that in non-infected mice after necropsy. (**D**) Viral loads (nLuc activity/mg) from indicated tissues using Vero E6 cells as targets. Virus loads in indicated tissues were determined when they succumbed to infection (dashed ellipse with red dagger, only for not 100% mortality cohorts) and at 20 dpi for surviving mice. Grouped data in (B-D) were analyzed by 2-way ANOVA followed by Tukey's multiple comparison tests. Statistical significance for group comparisons to control are shown in black, M58 (prophylaxis) in purple, M81 (prophylaxis) in blue, M58 (therapy) in red and M81(therapy)

in green. Non-significant comparison is not shown. $*$, $P < 0.05$; $**$, $P < 0.01$; $***$, $P < 0.001$; Mean values ± SD are depicted.

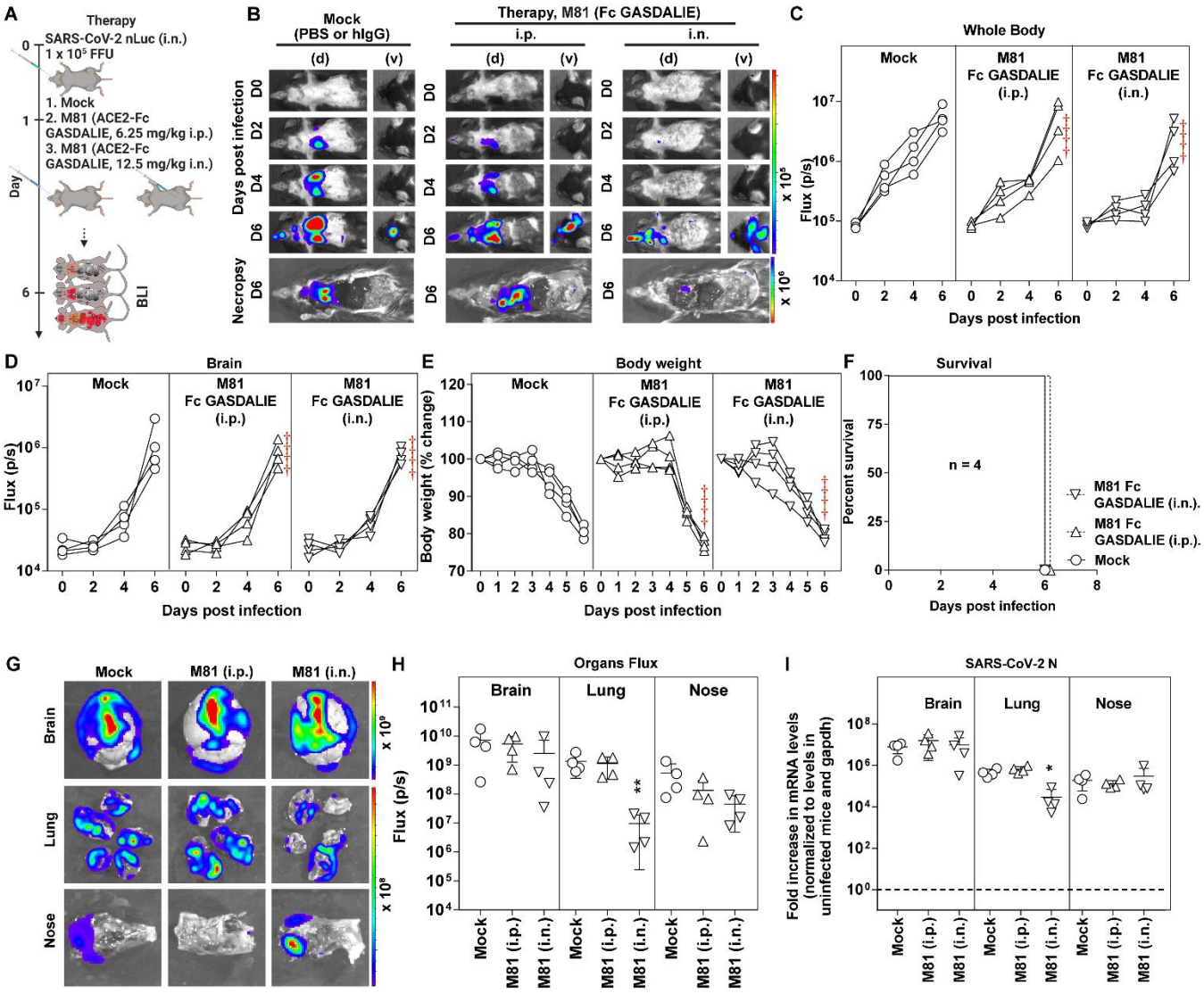

Fig. S11. Single mucosal or peripheral administration of M81 during therapy does not protect mice against lethal SARS-CoV-2 infection in mice

(**A**) A scheme showing experimental design for testing *in vivo* efficacy of M81 ($ACE2_{740}$ LFMYQY2HA-Fc GASDALIE) when delivered either intranasally (*i.n.*, 12.5 mg/kg) or intraperitoneally (*i.p.*, 6.25 mg/kg) 1 day after (+1 dpi, therapy) challenging K18-hACE2 mice with 1 x 10^5 FFU SARS-CoV-2-nLuc. PBS-treated mice (n=4) were used as control. (**B**) Representative BLI images of SARS-CoV-2-nLuc-infected mice in ventral (v) and dorsal (d)

positions. Images of dorsal views show the head to demonstrate virus neuroinvasion. (**C-D**) Temporal quantification of nLuc signal as flux (photons/sec) computed non-invasively. (**E**) Temporal changes in mouse body weight with initial body weight set to 100% for an experiment shown in A. Mice that succumb to infection are denoted with red daggers. (**F**) Kaplan-Meier survival curves of mice (n = 4 per group) statistically compared by log-rank (Mantel-Cox). (**G-H**) *Ex vivo* imaging of indicated organs and quantification of nLuc signal as flux (photons/sec) after necropsy. (**I**) Fold changes in nucleocapsid mRNA expression in brain, lung and nasal cavity tissues. Data were normalized to *Gapdh* mRNA in the same sample and that in non-infected mice after necropsy. Grouped data in (H-I) were analyzed by 2-way ANOVA followed by Tukey's multiple comparison tests. $*$, $p < 0.05$; $**$, $p < 0.01$; Mean values ± SD are depicted.

REFERENCES AND NOTES

1. A. N. Vlasova, A. Diaz, D. Damtie, L. Xiu, T.-H. Toh, J. S.-Y. Lee, L. J. Saif, G. C. Gray, Novel canine coronavirus isolated from a hospitalized patient with pneumonia in East Malaysia. *Clin. Infect. Dis.* **74**, 446–454 (2022).

2. Z. A. Abdulla, S. M. Al-Bashir, N. S. Al-Salih, A. A. Aldamen, M. Z. Abdulazeez, A summary of the SARS-CoV-2 vaccines and technologies available or under development. *Pathogens* **10**, 788 (2021).

3. W. T. Harvey, A. M. Carabelli, B. Jackson, R. K. Gupta, E. C. Thomson, E. M. Harrison, C. Ludden, R. Reeve, A. Rambaut; COVID-19 GENOMICS UK (COG-UK) Consortium, S. J. Peacock, D. L. Robertson, SARS-CoV-2 variants, spike mutations and immune escape. *Nat. Rev. Microbiol.* **19**, 409–424 (2021).

4. D. Wrapp, N. Wang, K. S. Corbett, J. A. Goldsmith, C.-L. Hsieh, O. Abiona, B. S. Graham, J. S. McLellan, Cryo-EM structure of the 2019-nCoV spike in the prefusion conformation. *Science* **367**, 1260–1263 (2020).

5. A. C. Walls, M. A. Tortorici, J. Snijder, X. Xiong, B.-J. Bosch, F. A. Rey, D. Veesler, Tectonic conformational changes of a coronavirus spike glycoprotein promote membrane fusion. *Proc. Natl. Acad. Sci. U.S.A.* **114**, 11157–11162 (2017).

6. R. Yan, Y. Zhang, Y. Li, L. Xia, Y. Guo, Q. Zhou, Structural basis for the recognition of the SARS-CoV-2 by full-length human ACE2. *Science* **367**, 1444–1448 (2020).

7. C. Tikellis, M. C. Thomas, Angiotensin-converting enzyme 2 (ACE2) is a key modulator of the renin angiotensin system in health and disease. *Int. J. Pept.* **2012**, 256294 (2012).

8. V. Monteil, H. Kwon, P. Prado, A. Hagelkrüys, R. A. Wimmer, M. Stahl, A. Leopoldi, E. Garreta, C. H. Del Pozo, F. Prosper, J. P. Romero, G. Wirnsberger, H. Zhang, A. S. Slutsky, R. Conder, N. Montserrat, A. Mirazimi, J. M. Penninger, Inhibition of SARS-CoV-2 infections in engineered human tissues using clinical-grade soluble human ACE2. *Cell* **181**, 905–913.e7 (2020).

9. D. Batlle, J. Wysocki, K. Satchell, Soluble angiotensin-converting enzyme 2: A potential approach for coronavirus infection therapy? *Clin. Sci. (Lond.)* **134**, 543–545 (2020).

10. A. Zoufaly, M. Poglitsch, J. H. Aberle, W. Hoepler, T. Seitz, M. Traugott, A. Grieb, E. Pawelka, H. Laferl, C. Wenisch, S. Neuhold, D. Haider, K. Stiasny, A. Bergthaler, E. Puchhammer-Stoeckl, A. Mirazimi, N. Montserrat, H. Zhang, A. S. Slutsky, J. M. Penninger, Human recombinant soluble ACE2 in severe COVID-19. *Lancet Respir. Med.* **8**, 1154–1158 (2020).

11. T. Yamaguchi, M. Hoshizaki, T. Minato, S. Nirasawa, M. N. Asaka, M. Niiyama, M. Imai, A. Uda, J. F.-W. Chan, S. Takahashi, J. An, A. Saku, R. Nukiwa, D. Utsumi, M. Kiso, A. Yasuhara, V. K.-M. Poon, C. C.-S. Chan, Y. Fujino, S. Motoyama, S. Nagata, J. M. Penninger, H. Kamada, K.-Y. Yuen, W. Kamitani, K. Maeda, Y. Kawaoka, Y. Yasutomi, Y. Imai, K. Kuba, ACE2-like carboxypeptidase B38-CAP protects from SARS-CoV-2-induced lung injury. *Nat. Commun.* **12**, 6791 (2021).

12. K. Kuba, Y. Imai, S. Rao, H. Gao, F. Guo, B. Guan, Y. Huan, P. Yang, Y. Zhang, W. Deng, L. Bao, B. Zhang, G. Liu, Z. Wang, M. Chappell, Y. Liu, D. Zheng, A. Leibbrandt, T. Wada, A. S. Slutsky, D. Liu, C. Qin, C. Jiang, J. M. Penninger, A crucial role of angiotensin converting enzyme 2 (ACE2) in SARS coronavirus-induced lung injury. *Nat. Med.* **11**, 875–879 (2005).

13. A. Glasgow, J. Glasgow, D. Limonta, P. Solomon, I. Lui, Y. Zhang, M. A. Nix, N. J. Rettko, S. Zha, R. Yamin, K. Kao, O. S. Rosenberg, J. V. Ravetch, A. P. Wiita, K. K. Leung, S. A. Lim, X. X. Zhou, T. C. Hobman, T. Kortemme, J. A. Wells, Engineered ACE2 receptor traps potently neutralize SARS-CoV-2. *Proc. Natl. Acad. Sci. U.S.A.* **117**, 28046–28055 (2020).

14. K. K. Chan, D. Dorosky, P. Sharma, S. A. Abbasi, J. M. Dye, D. M. Kranz, A. S. Herbert, E. Procko, Engineering human ACE2 to optimize binding to the spike protein of SARS coronavirus 2. *Science* **369**, 1261–1265 (2020).

15. Y. Higuchi, T. Suzuki, T. Arimori, N. Ikemura, E. Mihara, Y. Kirita, E. Ohgitani, O. Mazda, D. Motooka, S. Nakamura, Y. Sakai, Y. Itoh, F. Sugihara, Y. Matsuura, S. Matoba, T. Okamoto, J. Takagi, A. Hoshino, Engineered ACE2 receptor therapy overcomes mutational escape of SARS-CoV-2. *Nat. Commun.* **12**, 3802 (2021).

16. K. K. Chan, T. J. C. Tan, K. K. Narayanan, E. Procko, An engineered decoy receptor for SARS-CoV-2 broadly binds protein S sequence variants. *Sci. Adv.* **7**, eabf1738 (2021).

17. B. Havranek, K. K. Chan, A. Wu, E. Procko, S. M. Islam, Computationally designed ACE2 decoy receptor binds SARS-CoV-2 spike (S) protein with tight nanomolar affinity. *J. Chem. Inf. Model.* **61**, 4656–4669 (2021).

18. L. Hassler, J. Wysocki, I. Gelarden, I. Sharma, A. Tomatsidou, M. Ye, H. Gula, V. Nicoleascu, G. Randall, S. Pshenychnyi, N. Khurram, Y. Kanwar, D. Missiakas, J. Henkin, A. Yeldandi, D. Batlle, A novel soluble ACE2 protein provides lung and kidney protection in mice susceptible to lethal SARS-CoV-2 infection. *J. Am. Soc. Nephrol.* ASN.2021091209 (2022).

19. T. Xiao, J. Lu, J. Zhang, R. I. Johnson, L. G. A. McKay, N. Storm, C. L. Lavine, H. Peng, Y. Cai, S. Rits-Volloch, S. Lu, B. D. Quinlan, M. Farzan, M. S. Seaman, A. Griffiths, B. Chen, A trimeric human angiotensin-converting enzyme 2 as an anti-SARS-CoV-2 agent. *Nat. Struct. Mol. Biol.* **28**, 202–209 (2021).

20. A. Miller, A. Leach, J. Thomas, C. McAndrew, E. Bentley, G. Mattiuzzo, L. John, A. Mirazimi, G. Harris, N. Gamage, S. Carr, H. Ali, R. van Montfort, T. Rabbitts, A super-potent tetramerized ACE2 protein displays enhanced neutralization of SARS-CoV-2 virus infection. *Sci. Rep.* **11**, 10617 (2021).

21. L. Cao, I. Goreshnik, B. Coventry, J. B. Case, L. Miller, L. Kozodoy, R. E. Chen, L. Carter, A. C. Walls, Y.-J. Park, E.-M. Strauch, L. Stewart, M. S. Diamond, D. Veesler, D. Baker, De novo design of picomolar SARS-CoV-2 miniprotein inhibitors. *Science* **370**, 426–431 (2020).

22. J. M. Inal, Decoy ACE2-expressing extracellular vesicles that competitively bind SARS-CoV-2 as a possible COVID-19 therapy. *Clin. Sci. (Lond.)* **134**, 1301–1304 (2020).

23. J. Lan, J. Ge, J. Yu, S. Shan, H. Zhou, S. Fan, Q. Zhang, X. Shi, Q. Wang, L. Zhang, X. Wang, Structure of the SARS-CoV-2 spike receptor-binding domain bound to the ACE2 receptor. *Nature* **581**, 215–220 (2020).

24. J. Shang, G. Ye, K. Shi, Y. Wan, C. Luo, H. Aihara, Q. Geng, A. Auerbach, F. Li, Structural basis of receptor recognition by SARS-CoV-2. *Nature* **581**, 221–224 (2020).

25. T. H. Chu, A. R. Crowley, I. Backes, C. Chang, M. Tay, T. Broge, M. Tuyishime, G. Ferrari, M. S. Seaman, S. I. Richardson, G. D. Tomaras, G. Alter, D. Leib, M. E. Ackerman, Hinge length contributes to the phagocytic activity of HIV-specific IgG1 and IgG3 antibodies. *PLOS Pathog.* **16**, e1008083 (2020).

26. S. I. Richardson, B. E. Lambson, A. R. Crowley, A. Bashirova, C. Scheepers, N. Garrett, S. Abdool Karim, N. N. Mkhize, M. Carrington, M. E. Ackerman, P. L. Moore, L. Morris, IgG3 enhances neutralization potency and Fc effector function of an HIV V2-specific broadly neutralizing antibody. *PLOS Pathog.* **15**, e1008064 (2019).

27. S. E. Butler, A. R. Crowley, H. Natarajan, S. Xu, J. A. Weiner, C. A. Bobak, D. E. Mattox, J. Lee, W. Wieland-Alter, R. I. Connor, P. F. Wright, M. E. Ackerman, Distinct features and functions of systemic and mucosal humoral immunity among SARS-CoV-2 convalescent individuals. *Front. Immunol.* **11**, 618685 (2021).

28. E. P. Barros, L. Casalino, Z. Gaieb, A. C. Dommer, Y. Wang, L. Fallon, L. Raguette, K. Belfon, C. Simmerling, R. E. Amaro, The flexibility of ACE2 in the context of SARS-CoV-2 infection. *Biophys. J.* **120**, 1072–1084 (2021).

29. S. R. Leist, K. H. Dinnon III, A. Schäfer, L. V. Tse, K. Okuda, Y. J. Hou, A. West, C. E. Edwards, W. Sanders, E. J. Fritch, K. L. Gully, T. Scobey, A. J. Brown, T. P. Sheahan, N. J. Moorman, R. C. Boucher, L. E. Gralinski, S. A. Montgomery, R. S. Baric, A mouse-adapted SARS-CoV-2 induces acute lung injury and mortality in standard laboratory mice. *Cell* **183**, 1070–1085.e12 (2020).

30. P. Towler, B. Staker, S. G. Prasad, S. Menon, J. Tang, T. Parsons, D. Ryan, M. Fisher, D. Williams, N. A. Dales, M. A. Patane, M. W. Pantoliano, ACE2 X-ray structures reveal a large hinge-bending motion important for inhibitor binding and catalysis. *J. Biol. Chem.* **279**, 17996–18007 (2004).

31. S. L. Chen, T. Marino, W. H. Fang, N. Russo, F. Himo, Peptide hydrolysis by the binuclear zinc enzyme aminopeptidase from Aeromonas proteolytica: A density functional theory study. *J. Phys. Chem. B* **112**, 2494–2500 (2008).

32. C. Lei, K. Qian, T. Li, S. Zhang, W. Fu, M. Ding, S. Hu, Neutralization of SARS-CoV-2 spike pseudotyped virus by recombinant ACE2-Ig. *Nat. Commun.* **11**, 2070 (2020).

33. D. J. Benton, A. G. Wrobel, C. Roustan, A. Borg, P. Xu, S. R. Martin, P. B. Rosenthal, J. J. Skehel, S. J. Gamblin, The effect of the D614G substitution on the structure of the spike glycoprotein of SARS-CoV-2. *Proc. Natl. Acad. Sci. U.S.A.* **118**, e2022586118 (2021).

34. S. Ozono, Y. Zhang, H. Ode, K. Sano, T. S. Tan, K. Imai, K. Miyoshi, S. Kishigami, T. Ueno, Y. Iwatani, T. Suzuki, K. Tokunaga, SARS-CoV-2 D614G spike mutation increases entry efficiency with enhanced ACE2-binding affinity. *Nat. Commun.* **12**, 848 (2021).

35. L. Niu, K. N. Wittrock, G. C. Clabaugh, V. Srivastava, M. W. Cho, A structural landscape of neutralizing antibodies against SARS-CoV-2 receptor binding domain. *Front. Immunol.* **12**, 647934 (2021).

36. S. H. Tseng, B. Lam, Y. J. Kung, J. Lin, L. Liu, Y. C. Tsai, L. Ferrall, R. B. S. Roden, T. C. Wu, C.F. Hung, A novel pseudovirus-based mouse model of SARS-CoV-2 infection to test COVID-19 interventions. *J. Biomed. Sci.* **28**, 34 (2021).

37. K. H. D. Crawford, R. Eguia, A. S. Dingens, A. N. Loes, K. D. Malone, C. R. Wolf, H. Y. Chu, M. A. Tortorici, D. Veesler, M. Murphy, D. Pettie, N. P. King, A. B. Balazs, J. D. Bloom, Protocol and reagents for pseudotyping lentiviral particles with SARS-CoV-2 spike protein for neutralization assays. *Viruses* **12**, 513 (2020).

38. G. Beaudoin-Bussieres, J. Richard, J. Prevost, G. Goyette, A. Finzi, A new flow cytometry assay to measure antibody-dependent cellular cytotoxicity against SARS-CoV-2 Spike-expressing cells. *STAR Protoc.* **2**, 100851 (2021).

39. S. Fischinger, J. K. Fallon, A. R. Michell, T. Broge, T. J. Suscovich, H. Streeck, G. Alter, A high-throughput, bead-based, antigen-specific assay to assess the ability of antibodies to induce complement activation. *J. Immunol. Methods* **473**, 112630 (2019).

40. M. Lo, H. S. Kim, R. K. Tong, T. W. Bainbridge, J.-M. Vernes, Y. Zhang, Y. L. Lin, S. Chung, M. S. Dennis, Y. J. Y. Zuchero, R. J. Watts, J. A. Couch, Y. G. Meng, J. K. Atwal, R. J. Brezski, C. Spiess, J. A. Ernst, Effector-attenuating substitutions that maintain antibody stability and reduce toxicity in mice. *J. Biol. Chem.* **292**, 3900–3908 (2017).

41. M. E. Ackerman, B. Moldt, R. T. Wyatt, A.-S. Dugast, E. McAndrew, S. Tsoukas, S. Jost, C. T. Berger, G. Sciaranghella, Q. Liu, D. J. Irvine, D. R. Burton, G. Alter, A robust, high-throughput assay to determine the phagocytic activity of clinical antibody samples. *J. Immunol. Methods* **366**, 8–19 (2011).

42. S. M. S. Cheng, C. K. P. Mok, Y. W. Y. Leung, S. S. Ng, K. C. K. Chan, F. W. Ko, C. Chen, K. Yiu, B. H. S. Lam, E. H. Y. Lau, K. K. P. Chan, L. L. H. Luk, J. K. C. Li, L. C. H. Tsang, L. L. M. Poon, D. S. C. Hui, M. Peiris, Neutralizing antibodies against the SARS-CoV-2 Omicron variant BA.1 following homologous and heterologous CoronaVac or BNT162b2 vaccination. *Nat. Med.* **28**, 486–489 (2022).

43. H. Shuai, J. F.-W. Chan, B. Hu, Y. Chai, T. T.-T. Yuen, F. Yin, X. Huang, C. Yoon, J.-C. Hu, H. Liu, J. Shi, Y. Liu, T. Zhu, J. Zhang, Y. Hou, Y. Wang, L. Lu, J.-P. Cai, A. J. Zhang, J. Zhou, S. Yuan, M. A. Brindley, B.-Z. Zhang, J.-D. Huang, K. K.-W. To, K.-Y. Yuen, H. Chu, Attenuated replication and pathogenicity of SARS-CoV-2 B.1.1.529 Omicron. *Nature* **603**, 693–699 (2022).

44. J. Wysocki, M. Ye, L. Hassler, A. K. Gupta, Y. Wang, V. Nicoleascu, G. Randall, J. A. Wertheim, D. Batlle, A novel soluble ACE2 variant with prolonged duration of action neutralizes SARS-CoV-2 infection in human kidney organoids. *J. Am. Soc. Nephrol.* **32**, 795–803 (2021).

45. Z. Zhang, E. Zeng, L. Zhang, W. Wang, Y. Jin, J. Sun, S. Huang, W. Yin, J. Dai, Z. Zhuang, Z. Chen, J. Sun, A. Zhu, F. Li, W. Cao, X. Li, Y. Shi, M. Gan, S. Zhang, P. Wei, J. Huang, N. Zhong, G. Zhong, J. Zhao, Y. Wang, W. Shao, J. Zhao, Potent prophylactic and therapeutic efficacy of recombinant human ACE2-Fc against SARS-CoV-2 infection in vivo. *Cell Discov.* **7**, 65 (2021).

46. L. Zhang, S. Dutta, S. Xiong, M. Chan, K. K. Chan, T. M. Fan, K. L. Bailey, M. Lindeblad, L. M. Cooper, L. Rong, A. F. Gugliuzza, D. Shukla, E. Procko, J. Rehman, A. B. Malik, Engineered ACE2 decoy mitigates lung injury and death induced by SARS-CoV-2 variants. *Nat. Chem. Biol.* **18**, 342–351 (2022).

47. D. Zipeto, J. D. F. Palmeira, G. A. Arganaraz, E. R. Arganaraz, ACE2/ADAM17/TMPRSS2 interplay may be the main risk factor for COVID-19. *Front. Immunol.* **11**, 576745 (2020).

48. M. J. Moore, T. Dorfman, W. Li, S. K. Wong, Y. Li, J. H. Kuhn, J. Coderre, N. Vasilieva, Z. Han, T. C. Greenough, M. Farzan, H. Choe, Retroviruses pseudotyped with the severe acute respiratory syndrome coronavirus spike protein efficiently infect cells expressing angiotensin-converting enzyme 2. *J. Virol.* **78**, 10628–10635 (2004).

49. N. Iwanaga, L. Cooper, L. Rong, B. Beddingfield, J. Crabtree, R. A. Tripp, X. Qin, J. K. Kolls, Novel ACE2-IgG1 fusions with improved *in vitro* and *in vivo* activity against SARS-CoV2. bioRxiv 2020.06.15.152157 [**Preprint**]. 24 July 2020. https://doi.org/10.1101/2020.06.15.152157.

50. K. O. Saunders, Conceptual approaches to modulating antibody effector functions and circulation half-life. *Front. Immunol.* **10**, 1296 (2019).

51. F. S. Oladunni, J.-G. Park, P. A. Pino, O. Gonzalez, A. Akhter, A. Allué-Guardia, A. Olmo-Fontánez, S. Gautam, A. Garcia-Vilanova, C. Ye, K. Chiem, C. Headley, V. Dwivedi, L. M. Parodi, K. J. Alfson, H. M. Staples, A. Schami, J. I. Garcia, A. Whigham, R. N. Platt II, M. Gazi, J. Martinez, C. Chuba, S. Earley, O. H. Rodriguez, S. D. Mdaki, K. N. Kavelish, R. Escalona, C. R. A. Hallam, C. Christie, J. L. Patterson, T. J. C. Anderson, R. Carrion Jr, E. J. Dick Jr, S. Hall-Ursone, L. S. Schlesinger, X. Alvarez, D. Kaushal, L. D. Giavedoni, J. Turner, L. Martinez-Sobrido, J. B. Torrelles, Lethality of SARS-CoV-2 infection in K18 human angiotensin-converting enzyme 2 transgenic mice. *Nat. Commun.* **11**, 6122 (2020).

52. P. B. McCray Jr., L. Pewe, C. Wohlford-Lenane, M. Hickey, L. Manzel, L. Shi, J. Netland, H. P. Jia, C. Halabi, C. D. Sigmund, D. K. Meyerholz, P. Kirby, D. C. Look, S. Perlman, Lethal infection of K18-hACE2 mice infected with severe acute respiratory syndrome coronavirus. *J. Virol.* **81**, 813–821 (2007).

53. I. Ullah, J. Prévost, M. S. Ladinsky, H. Stone, M. Lu, S. P. Anand, G. Beaudoin-Bussières, K. Symmes, M. Benlarbi, S. Ding, R. Gasser, C. Fink, Y. Chen, A. Tauzin, G. Goyette, C. Bourassa, H. Medjahed, M. Mack, K. Chung, C. B. Wilen, G. A. Dekaban, J. D. Dikeakos, E. A. Bruce, D. E. Kaufmann, L. Stamatatos, A. T. McGuire, J. Richard, M. Pazgier, P. J. Bjorkman, W. Mothes, A. Finzi, P. Kumar, P. D. Uchil, Live imaging of SARS-CoV-2 infection in mice reveals that neutralizing antibodies require Fc function for optimal efficacy. *Immunity* **54**, 2143–2158.e15 (2021).

54. G. Beaudoin-Bussieres, Y. Chen, I. Ullah, J. Prévost, W. D. Tolbert, K. Symmes, S. Ding, M. Benlarbi, S. Y. Gong, A. Tauzin, R. Gasser, D. Chatterjee, D. Vézina, G. Goyette, J. Richard, F. Zhou, L. Stamatatos, A. T. McGuire, H. Charest, M. Roger, E. Pozharski, P. Kumar, W. Mothes, P. D. Uchil, M. Pazgier, A. Finzi, A Fc-enhanced NTD-binding non-neutralizing antibody delays virus spread and synergizes with a nAb to protect mice from lethal SARS-CoV-2 infection. *Cell Rep.* **38**, 110368 (2022).

55. W. S. Lee, A. K. Wheatley, S. J. Kent, B. J. DeKosky, Antibody-dependent enhancement and SARS-CoV-2 vaccines and therapies. *Nat. Microbiol.* **5**, 1185–1191 (2020).

56. S. Wang, J. Wang, X. Yu, W. Jiang, S. Chen, R. Wang, M. Wang, S. Jiao, Y. Yang, W. Wang, H. Chen, B. Chen, C. Gu, C. Liu, A. Wang, M. Wang, G. Li, C. Guo, D. Liu, J. Zhang, M. Zhang, L. Wang, X. Gui, Antibody-dependent enhancement (ADE) of SARS-CoV-2 pseudoviral infection requires FcγRIIB and virus-antibody complex with bivalent interaction. *Commun. Biol.* **5**, 262 (2022).

57. Y. Liu, W. T. Soh, J.-I. Kishikawa, M. Hirose, E. E. Nakayama, S. Li, M. Sasai, T. Suzuki, A. Tada, A. Arakawa, S. Matsuoka, K. Akamatsu, M. Matsuda, C. Ono, S. Torii, K. Kishida, H. Jin, W. Nakai, N. Arase, A. Nakagawa, M. Matsumoto, Y. Nakazaki, Y. Shindo, M. Kohyama, K. Tomii, K. Ohmura, S. Ohshima, T. Okamoto, M. Yamamoto, H. Nakagami, Y. Matsuura, A. Nakagawa, T. Kato, M. Okada, D. M. Standley, T. Shioda, H. Arase, An infectivity-enhancing site on the SARS-CoV-2 spike protein targeted by antibodies. *Cell* **184**, 3452–3466.e18 (2021).

58. D. Li, R. J. Edwards, K. Manne, D. R. Martinez, A. Schäfer, S. M. Alam, K. Wiehe, X. Lu, R. Parks, L. L. Sutherland, T. H. Oguin III, C. M. Danal, L. G. Perez, K. Mansouri, S. M. C. Gobeil, K.

Janowska, V. Stalls, M. Kopp, F. Cai, E. Lee, A. Foulger, G. E. Hernandez, A. Sanzone, K. Tilahun, C. Jiang, L. V. Tse, K. W. Bock, M. Minai, B. M. Nagata, K. Cronin, V. Gee-Lai, M. Deyton, M. Barr, T. V. Holle, A. N. Macintyre, E. Stover, J. Feldman, B. M. Hauser, T. M. Caradonna, T. D. Scobey, W. Rountree, Y. Wang, M. A. Moody, D. W. Cain, C. T. De Marco, T. N. Denny, C. W. Woods, E. W. Petzold, A. G. Schmidt, I.-T. Teng, T. Zhou, P. D. Kwong, J. R. Mascola, B. S. Graham, I. N. Moore, R. Seder, H. Andersen, M. G. Lewis, D. C. Montefiori, G. D. Sempowski, R. S. Baric, P. Acharya, B. F. Haynes, K. O. Saunders, In vitro and in vivo functions of SARS-CoV-2 infection-enhancing and neutralizing antibodies. *Cell* **184**, 4203–4219.e32 (2021).

59. L. Zhang, K. K. Narayanan, L. Cooper, K. K. Chan, C. A. Devlin, A. Aguhob, K. Shirley, L. Rong, J. Rehman, A. B. Malik, E. Procko, An engineered ACE2 decoy receptor can be administered by inhalation and potently targets the BA.1 and BA.2 omicron variants of SARS-CoV-2. bioRxiv 2022.03.28.486075 [Preprint]. 28 March 2022. https://doi.org/10.1101/2022.03.28.486075.

60. C.-L. Hsieh, J. A. Goldsmith, J. M. Schaub, A. M. DiVenere, H.-C. Kuo, K. Javanmardi, K. C. le, D. Wrapp, A. G. Lee, Y. Liu, C.-W. Chou, P. O. Byrne, C. K. Hjorth, N. V. Johnson, J. Ludes-Meyers, A. W. Nguyen, J. Park, N. Wang, D. Amengor, J. J. Lavinder, G. C. Ippolito, J. A. Maynard, I. J. Finkelstein, J. S. McLellan, Structure-based design of prefusion-stabilized SARS-CoV-2 spikes. *Science* **369**, 1501–1505 (2020).

61. R. Sherburn, W. D. Tolbert, S. Gottumukkala, A. P. Hederman, G. Beaudoin-Bussières, S. Stanfield-Oakley, M. Tuyishime, G. Ferrari, A. Finzi, M. E. Ackerman, M. Pazgier, Incorporating the cluster A and V1V2 targets into a minimal structural unit of the HIV-1 envelope to elicit a cross-clade response with potent Fc-effector functions. *Vaccines (Basel)* **9**, 975 (2021).

62. W. Minor, M. Cymborowski, Z. Otwinowski, M. Chruszcz, HKL-3000: The integration of data reduction and structure solution—From diffraction images to an initial model in minutes. *Acta Crystallogr. D Biol. Crystallogr.* **62**, 859–866 (2006).

63. M. D. Winn, C. C. Ballard, K. D. Cowtan, E. J. Dodson, P. Emsley, P. R. Evans, R. M. Keegan, E. B. Krissinel, A. G. W. Leslie, A. McCoy, S. J. McNicholas, G. N. Murshudov, N. S. Pannu, E. A. Potterton, H. R. Powell, R. J. Read, A. Vagin, K. S. Wilson, Overview of the CCP4 suite and current developments. *Acta Crystallogr. D Biol. Crystallogr.* **67**, 235–242 (2011).

64. D. Liebschner, P. V. Afonine, M. L. Baker, G. Bunkóczi, V. B. Chen, T. I. Croll, B. Hintze, L. W. Hung, S. Jain, A. McCoy, N. W. Moriarty, R. D. Oeffner, B. K. Poon, M. G. Prisant, R. J. Read, J. S. Richardson, D. C. Richardson, M. D. Sammito, O. V. Sobolev, D. H. Stockwell, T. C. Terwilliger, A. G. Urzhumtsev, L. L. Videau, C. J. Williams, P.D. Adams, Macromolecular structure determination using X-rays, neutrons and electrons: Recent developments in Phenix. *Acta Crystallogr. D Struct. Biol.* **75**, 861–877 (2019).

65. P. Liu, J. Wysocki, P. Serfozo, M. Ye, T. Souma, D. Batlle, J. Jin, A fluorometric method of measuring carboxypeptidase activities for angiotensin II and apelin-13. *Sci. Rep.* **7**, 45473 (2017).

66. F. Ferrara, N. Temperton, Pseudotype neutralization assays: From laboratory bench to data analysis. *Methods Protoc.* **1**, 8 (2018).

67. H. Mou, B. D. Quinlan, H. Peng, G. Liu, Y. Guo, S. Peng, L. Zhang, M. E. Davis-Gardner, M. R. Gardner, G. Crynen, L. B. DeVaux, Z. X. Voo, C. C. Bailey, M. D. Alpert, C. Rader, M. U. Gack, H. Choe, M. Farzan, Mutations derived from horseshoe bat ACE2 orthologs enhance ACE2-Fc neutralization of SARS-CoV-2. *PLOS Pathog.* **17**, e1009501 (2021).

68. M. S. Weiss, Global indicators of X-ray data quality. *J. Appl. Cryst.* **34**, 130–135 (2001).

69. P. A. Karplus, K. Diederichs, Linking crystallographic model and data quality. *Science* **336**, 1030–1033 (2012).

70. A. N. Popov, G. P. Bourenkov, Choice of data-collection parameters based on statistic modelling. *Acta Crystallogr. D Biol. Crystallogr.* **59**, 1145–1153 (2003).

71. A. T. Brunger, Free R value: Cross-validation in crystallography. *Methods Enzymol.* **277**, 366–396 (1997).

72. V. B. Chen, W. B. Arendall III, J. J. Headd, D. A. Keedy, R. M. Immormino, G. J. Kapral, L. W. Murray, J. S. Richardson, D. C. Richardson, MolProbity: All-atom structure validation for macromolecular crystallography. *Acta Crystallogr. D Biol. Crystallogr.* **66**, 12–21 (2010).

73. Y. Liu, J. Liu, K. S. Plante, J. A. Plante, X. Xie, X. Zhang, Z. Ku, Z. An, D. Scharton, C. Schindewolf, V. D. Menachery, P.-Y. Shi, S. C. Weaver, The N501Y spike substitution enhances SARS-CoV-2 transmission. bioRxiv 2021.03.08.434499 [Preprint]. 9 March 2021. https://doi.org/10.1101/2021.03.08.434499.

74. J. Zalevsky, A.K. Chamberlain, H.M. Horton, S. Karki, I.W.L. Leung, T.J. Sproule, G.A. Lazar, D.C. Roopenian, J.R. Desjarlais, Enhanced antibody half-life improves in vivo activity. *Nat. Biotechnol.* **28**, 157–159 (2010).